The bearing strength perpendicular to the grain of locally loaded timber blocks and dowel-type connections

Ir. J.C.M. (Dennis) Schoenmakers
Eindhoven University of Technology, Eindhoven, the Netherlands

Abstract

In the past compression perpendicular to the grain is investigated and reported by many as for instance by Kollmann [6] and Augustin and Schickhofer [2]. Several attempts have been made to describe strength and deformation behaviour empirically. It is well known that timber loaded in compression perpendicular to the grain shows hardening, i.e. the initially linear stress-strain relation becomes non-linear after a certain deformation level (the material loses stiffness). Consequently, the local bearing strength increases strongly, associated with large deformations (plastic behaviour). To explain this phenomenon a theoretical-based model is presented while test results are used for validation. The theory however has been presented several times by Van der Put, Stevin report HSC-6 [9] as early as 1988 to explain the very high embedding strength of nailed particle board, and by Van der Put and Leijten [11] and more recently by Van der Put [10], in which test data are used for validation. It all confirms the theory to explain the perpendicular to grain compressive (bearing) strength very well, as described in Leijten and Schoenmakers [7] as well.

First this paper deals with the theoretical background and derivation of the model. Besides, the behaviour of locally loaded timber blocks in compression perpendicular to the grain is very similar to the bearing (embedment) behaviour of dowel-type fasteners. Therefore the theory is applicable on connection failure as well, see also Van der Put and Leijten [11] . This paper intends to contribute to the credibility of this model, and to show the prediction ability of both bearing blocks and bearing of dowel-type fasteners.

1 Introduction

The local compressive strength (bearing strength) perpendicular to the grain shows hardening due to restrained dilatation perpendicular to the grain, associated with a tri-axial stress state. This is explained and derived by Van der Put [10] with the equilibrium method of plasticity (slip-line field theory). The solution is derived using the method of characteristics. The high local strength appears to be dependant of the ability to spread (distribute) the load.

The slip-line field theory has shown to give exact solutions for plane deformation (strain) boundary value problems for rigid plastic solids. Besides equilibrium also the boundary conditions should be satisfied while stresses do not exceed a strength criterion. Sufficient plasticity should enable stress redistribution. The stress distribution chosen is the same as the one that follows from the slip-line theory, while another choice for the stress distribution is optional.

Below a timber block is loaded in compression perpendicular to the grain by two bearing plates. The block is loaded by a stress σ_s resulting in an opposite stress under the lower bearing plate equal to σ_o.

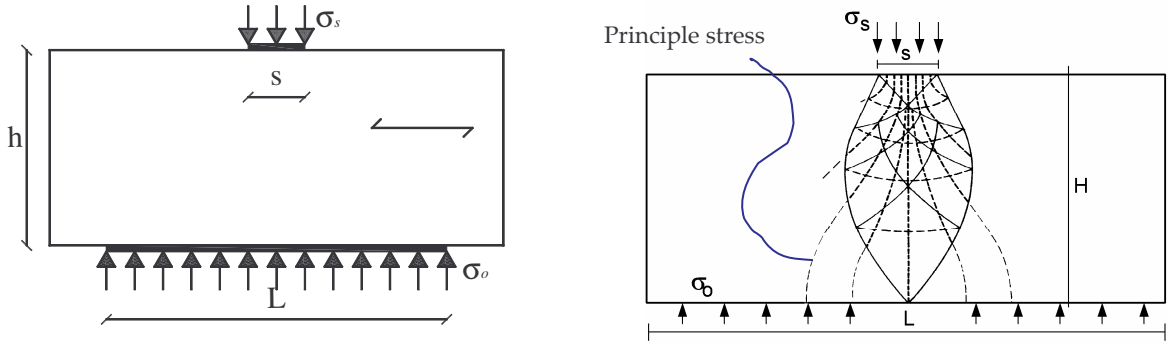

Figure 1: Compression test perpendicular to the grain, and assumed stress distribution

At failure the bearing strength, f_s, is reached just beneath the upper bearing plate. It appears that the bearing strength depends on the dimension of both plates. It is explained and derived by Van der Put [10] that the strength is proportional with the square root of the ratio between the loading area, dimensions s and t, and the supporting area, L t, where t is the constant width of the bearing block:

$$f_s = \mu\, f_{c;90} \sqrt{\frac{L\,t}{s\,t}} = 1.08\, f_{c;90} \sqrt{\frac{L}{s}} \qquad [\mathrm{N/mm^2}] \qquad (1.1)$$

The local bearing strength f_s thus increases with a factor 1.08 $\sqrt{(L/s)}$ compared to the standard compressive strength perpendicular to the grain, $f_{c;90}$. Apparently, the

ability to spread (distribute) the load and restrained dilatation in the material result in higher local strength values. In this situation the material is in a state of tri-axial compression.

The first application of the theory is given in 1988 (Van der Put, Stevin report HSC-6 [9]) and dealt with the embedment strength of nailed particle board. The validity of the theory was shown for timber as well. Comparison of Figures 1 and 2 shows that the behaviour is rather similar.

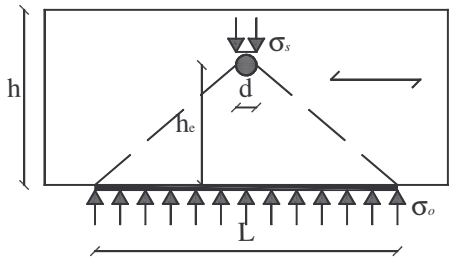

Figure 2: Dowel-type fastener loading the timber (embedment test)

Another interesting application is a dowel-type connection loading a timber beam away from the supports. Figure 3 shows this loading case to be a superposition of two simple cases. However, one needs to be aware that the model only predicts bearing (embedment) failure of the timber. Splitting failure is a completely different failure mechanism where fracture mechanical considerations result most probably in the best prediction model.

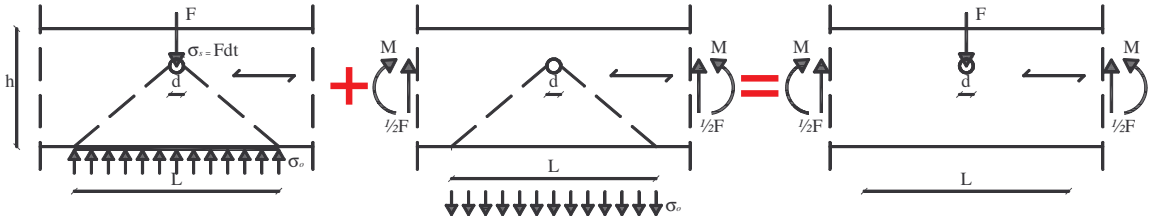

Figure 3: Dowel-type fastener loading a beam at mid span (right): superposition of stress states

2 Derivation of the bearing strength

The equilibrium method is used to solve the problem. Therefore, a stress field is constructed in the specimen that satisfies the equilibrium and the boundary conditions, and nowhere the stresses should exceed the failure criterion. It consists of a curvilinear mesh of two families of lines (stress trajectories) called the α-lines and the β-lines, which always intersect at right angels, see figure 4. By definition, the slip-lines are always parallel to the axis of principle shear stress. Since the shear stress is equal to the shear yield stress, k, the material evidently deforms by shear

parallel to the slip-lines, and therefore these lines are called slip-lines. If the slip-line field is constructed, the stresses can be calculated in every point using a set of partial differential equations, for which the method of characteristics is a common solution procedure. In certain cases the slip-lines are equal to the so-called characteristics of the set of equations, and this solution is the only correct one. Therefore, these particular slip-lines are called characteristics as well. The slip-line field theory is only applied to construct a stress field which is in accordance with equilibrium. It thus is irrelevant whether the material actually fails along these lines.

The next figure shows a small part of a slip-line field with the stress state for an infinitely small material part with dimensions dx dy. As the slip-lines are always parallel to the axis of principle shear stress, the normal stresses are always equal to p, which is the hydrostatic stress. The directions of the α- and β-lines are also given as dy/dx = tan(ψ+π/4) and dy/dx = tan(ψ-π/4). These angles are the angles corresponding to the (real) characteristics, as derived later.

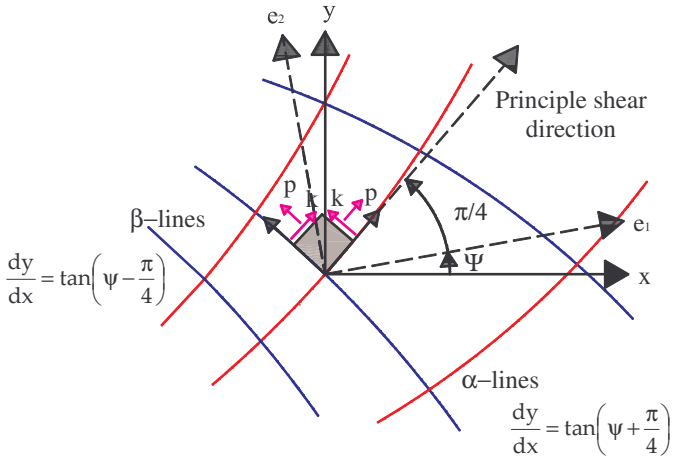

Figure 4: Detail of slip-line field

The equilibrium conditions are:

$$\frac{\partial \sigma_x}{\partial x} + \frac{\partial \tau}{\partial y} = 0 \qquad \text{and} \qquad \frac{\partial \sigma_y}{\partial y} + \frac{\partial \tau}{\partial x} = 0 \qquad (2.1)$$

A Tresca failure criterion is used, which applies after flow and hardening in the weak directions (RT and RL directions) until a quasi-isotropic flow occurs followed by further hardening and flow.

In Figure 5 the Tresca criterion is given in Mohr's circle with the general stress state σ_x, σ_y and τ_{xy}. The hydrostatic stress p is represented by the circle centre and thus is equal to the average of both principle stresses σ_1 en σ_2:

$$p = \frac{(\sigma_1 + \sigma_2)}{2} \qquad (2.2)$$

The failure criterion can be described with equation (2.3):

$$\frac{(\sigma_1 - \sigma_2)}{2} = k = f_v \qquad (2.3)$$

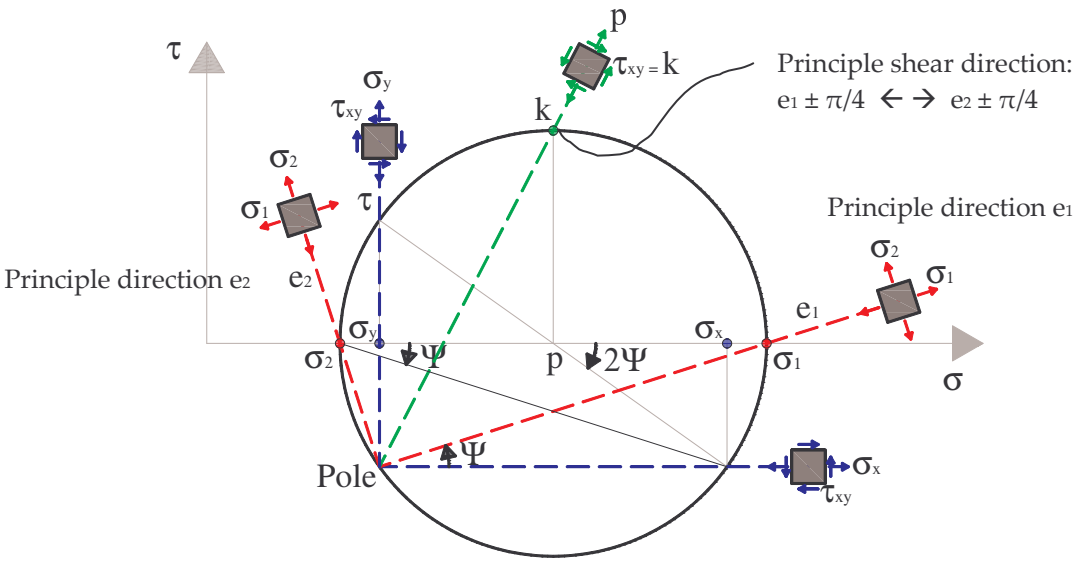

Figure 5: Circle of Mohr of the failure criterion

From this figure it can be noticed that the direction of the maximum shear stress differs $\pi/4$ from the principle directions, which corresponds with the directions of the slip-lines depicted in Figure 4. With the use of trigonometric relations the stresses σ_x, σ_y and τ_{xy} can be determined:

$$\sigma_y = p - k\cos 2\psi \qquad (2.4$$

$$\sigma_x = p + k\cos 2\psi \qquad (2.5$$

$$\tau = k\sin 2\psi \qquad (2.6)$$

The hydrostatic stress p can also be described using Cartesian stress components as follows:

$$p = \sigma_y + k \cos 2\psi = \sigma_x - k \cos 2\psi \qquad (2.7)$$

Substitution of the expressions for σ_x, σ_y and τ_{xy} in the equilibrium equations gives:

$$\frac{\partial p}{\partial x} - 2\,k \sin(2\psi)\frac{\partial \psi}{\partial x} + 2\,k \cos(2\psi)\frac{\partial \psi}{\partial y} = 0 \qquad (2.8)$$

$$\frac{\partial p}{\partial y} + 2\,k \cos(2\psi)\frac{\partial \psi}{\partial x} + 2\,k \sin(2\psi)\frac{\partial \psi}{\partial y} = 0 \qquad (2.9)$$

If equation (2.8) is multiplied with $\sin(\psi - \pi/4)$ and equation (2.9) with $\cos(\psi + \pi/4)$, addition of both equations is possible, which leads to the following relations (see also Schwarz [8] or Van der Put [10]) :

$$\frac{\partial(p - 2\,k\,\psi)}{\partial x} + \tan\left(\psi - \frac{\pi}{4}\right)\frac{\partial(p - 2\,k\,\psi)}{\partial y} = 0 \;\Rightarrow\; \frac{\partial a}{\partial x} + \tan\left(\psi - \frac{\pi}{4}\right)\frac{\partial a}{\partial y} = 0 \qquad (2.10)$$

$$\frac{\partial(p + 2\,k\,\psi)}{\partial x} + \tan\left(\psi + \frac{\pi}{4}\right)\frac{\partial(p + 2\,k\,\psi)}{\partial y} = 0 \;\Rightarrow\; \frac{\partial b}{\partial x} + \tan\left(\psi + \frac{\pi}{4}\right)\frac{\partial b}{\partial y} = 0 \qquad (2.11)$$

In order to obtain simplicity, two new variables, a and b, are defined, corresponding to α and β, belonging to both families of slip-lines. In equation (2.10), $a = p - 2\,k\psi$ (α -slip line). It follows that along the characteristic with slope $-dy/dx = \tan(\psi - \pi/4)$, "a" is a constant. In equation (2.11), $b = p + 2\,k\psi$ (β -slip line), and similarly, constant along the characteristic with slope $-dy/dx = \tan(\psi + \pi/4)$. Because dy/dx denote the directions, the negative sign "-" has no actual value, because it mirrors the specific angles with the horizontal axis.

Formally, it has to be proved that the slip-lines found are the true characteristics, and to do so, equations (2.8) and (2.9) are combined with their corresponding equations of variation (see Van der Put [10]):

$$\begin{pmatrix} 1 & 0 & -2\,k \sin 2\psi & 2\,k \cos 2\psi \\ 0 & 1 & 2\,k \cos 2\psi & 2\,k \sin 2\psi \\ 1 & \frac{dy}{dx} & 0 & 0 \\ 0 & 0 & 1 & \frac{dy}{dx} \end{pmatrix} \begin{Bmatrix} \frac{\partial p}{\partial x} \\ \frac{\partial p}{\partial y} \\ \frac{\partial \psi}{\partial x} \\ \frac{\partial \psi}{\partial y} \end{Bmatrix} = \begin{Bmatrix} 0 \\ 0 \\ \frac{dp}{dx} \\ \frac{d\psi}{dy} \end{Bmatrix} \qquad (2.12)$$

On the characteristics the derivatives have no determinate value and therefore all numerator and denominator determinants have to be zero in the characteristic directions. Accordingly, these directions can be found.

This is achieved using the method of characteristics solution procedure. A zero value of the numerator determinant gives, after subtracting the third row from the first (the first column and third row consist only of zeros and can be removed):

$$\det\begin{pmatrix} -\frac{dy}{dx} & -2\,k\sin 2\psi & 2\,k\cos 2\psi \\ 1 & 2\,k\cos 2\psi & 2\,k\sin 2\psi \\ 0 & 1 & \frac{dy}{dx} \end{pmatrix} = 0 \qquad (2.13)$$

Evaluation of this determinant gives:

$$-\left(\frac{dy}{dx}\right)^2 \cos 2\psi + 2\left(\frac{dy}{dx}\right)\sin 2\psi + \cos 2\psi = 0 \qquad (2.14)$$

Solving dy/dx results in the slopes of both orthogonal sets of characteristics:

$$\frac{dy}{dx} = \tan\left(\psi + \frac{\pi}{4}\right) \text{ (α-lines) and } \frac{dy}{dx} = \tan\left(\psi - \frac{\pi}{4}\right) \text{ (β-lines)} \qquad (2.15)$$

In this special case (symmetry) it follows that -dy/dx = tan (ψ - π/4) is equal to dy/dx = tan (ψ + π/4), corresponding to the α-family, as will be shown later. Similarly, -dy/dx = tan (ψ + π/4) is equal to dy/dx = tan (ψ - π/4) for the β-family.

A zero value of the denominator determinant gives:

$$\det\begin{pmatrix} -\frac{dy}{dx} & -2\,k\sin 2\psi & -\frac{dp}{dx} \\ 1 & 2\,k\cos 2\psi & 0 \\ 0 & 1 & \frac{d\psi}{dx} \end{pmatrix} = 0 \qquad (2.16)$$

Evaluation of this determinant gives:

$$-\frac{dy}{dx}\left(\frac{d\psi}{dx}\cos 2\psi\right) + \frac{d\psi}{dx}\sin 2\psi - \frac{1}{2\,k}\frac{dp}{dx} = 0 \qquad (2.17)$$

If equations (2.15) are substituted in equation (2.17), one obtains that $p \pm 2\,k\,\psi$ should be constant along the first respectively the second characteristic (the Hencky-relations, see Chakrabarty [3]):

$$p - 2\,k\,\psi = \text{constant along the } \alpha\text{-lines} \qquad (2.18)$$

$$p + 2\,k\,\psi = \text{constant along the } \beta\text{-lines} \qquad (2.19)$$

From the slopes of these lines it is concluded they are always perpendicular to each other as they should be. This relation was used before in order to derive equations (2.10) en (2.11). The constant value of $p \pm 2\,k\,\psi$ and the right angle between the lines proves that they are indeed characteristics.

In Figure 7 a small and simplified part of the entire mesh of slip-lines is depicted. Triangle AA*B is a region of constant stress state because a uniform compression load acts on the plane AA*. The maximum shear lines are therefore everywhere at $\pm$ 45° ($\pi/4$ radians) to the principle directions, and have to be straight. The directions of the characteristics were determined as $dy/dx = \tan(\psi \pm \pi/4)$, which shows that $\psi = \pi/2$ in this region, due to symmetry. In this case also the pole of Mohr's circle is located at point (σ_2, τ=0), which leads to $\psi = \pi/2$ as well. This direction of the plane with the principle stress is also the direction of the highest principle compression stress. This means that the Cartesian coordinate system makes right angles with the principle directions of stress e_1 and e_2. In order to maintain an x-axis which is horizontal, the coordinate systems are rotated, as depicted in Figure 6.

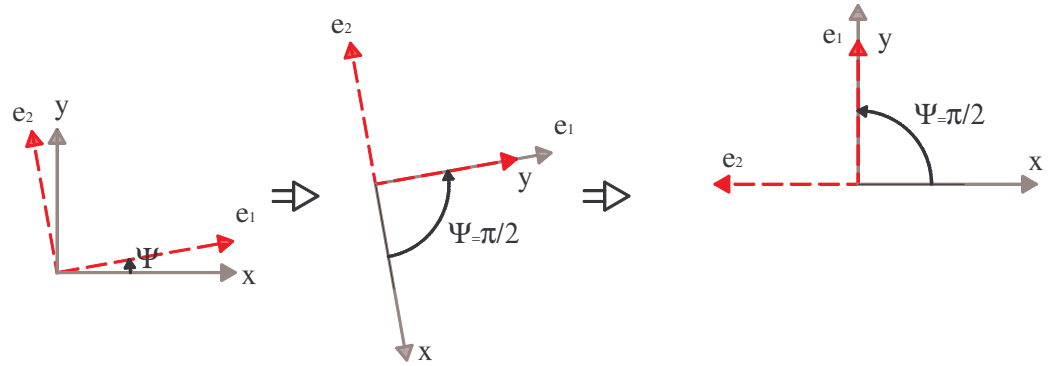

Figure 6: Rotation of principle axes and Cartesian axes to maintain horizontal x-axis

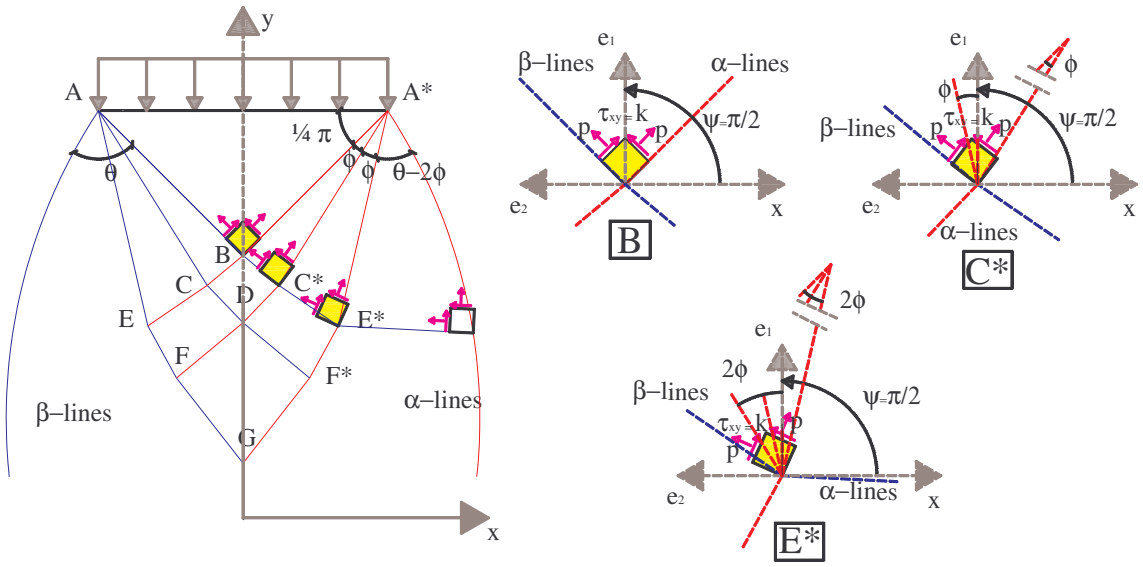

Figure 7: Sample of slip line field and detailed nodal information (crossings of slip-lines)

The mesh of slip-lines can now be computed, from point to point along a slip line as depicted in Figure 7. As this procedure can be quite time consuming, generally, this should be done numerically. As a starting point a point known from the boundary conditions should be taken. If one point is known, the next point can be calculated because of the geometric relations within the slip-line field. The real location of the intersection points is of minor interest, because these depend on the assumed angles ϕ with the principle shear axes. The stress state, however, is of interest. By definition, the maximum shear stress k is acting on each element but the hydrostatic stress p differs from point to point, as a result of changes in the element orientation.

In Figure 7 the curved slip-lines are represented by linear lines which approximate the curved ones, for simplification. Going from point B to point C* along the β-slip line ("+"-sign) with the use of the Hencky-equations given previously (angle measured counter clockwise):

$$p_B + 2k\frac{\pi}{2} = p_{C^*} + 2k\left(\frac{\pi}{2} + \phi\right) \quad \Rightarrow \quad p_{C^*} = p_B - 2k\phi \qquad (2.20)$$

Similarly, from point C* to point D, along the α-line ("-"-symbol):

$$p_{C^*} - 2k\left(\frac{\pi}{2} + \phi\right) = p_D - 2k\frac{\pi}{2} = \quad \Rightarrow \quad p_D = p_{C^*} - 2k\phi \qquad (2.21)$$

Substitution of p_{C^*} found in equation (2.20) in equation (2.21) yields:

$$p_D = p_{C^*} - 2\,k\,\phi = p_B - 2\,k\,\phi - 2\,k\,\phi \quad \Rightarrow \quad p_D = p_B - 4\,k\,\phi \qquad (2.22)$$

As a result of the constant compression state in triangle AA*B, the hydrostatic stress p_B must equal the compression load acting on plane AA*, thus $p_B = p_s$. By definition, the angle θ describes the angle between the first and last slip-line. As can be seen from Figure 7, $\theta = n\,\phi$, dependent of the number of ϕ-angles one wants to calculate. In general, the hydrostatic stress at the lower bearing plate p_o can thus be given in relation with the bearing stress at the upper plate:

$$p_o = p_s - 4\,k\,n\phi = p_s - 4\,k\,\theta \quad \Rightarrow \quad p_s = p_o + 4\,k\,\theta \qquad (2.23)$$

In Schwarz [8] the slip-lines are constructed numerically, and from this it follows that the angle θ follows from the logarithmic spiral shape of the characteristic, which can be approximated by the function:

$$\theta \approx 0.62\,\ln(2h/s) \qquad (2.24)$$

Substitution of θ in equation (2.23) yields:

$$p_s = p_o + 4\,k\,(0.62\,\ln(2h/s)) \qquad (2.25)$$

With Mohr's circle it follows that the principle compression stress σ_1 for the upper and lower bearing plates can be described as being the hydrostatic stress minus one time the shear strength k, so $p_i = \sigma_{1;i} - k$. It thus follows with equation (2.25):

$$\sigma_s - k = \sigma_o - k + 4\,k\,(0.62\,\ln(2h/s)) \quad \Rightarrow \quad \sigma_s = \sigma_o + 2.48\,k\,\ln(2h/s) \qquad (2.26)$$

In Figure 1 a compression test is depicted with the corresponding slip-line field, which thus determines the direction of the main stresses. Equilibrium of resultant forces yields:

$$\sigma_s\,s = \sigma_o\,L \quad \Rightarrow \quad \sigma_o = \frac{\sigma_s\,s}{L} \qquad (2.27)$$

It now follows from equation (2.27):

$$\sigma_s - \sigma_o = 2.48\,k\,\ln(2h/s) \quad \Rightarrow \quad \sigma_s - \frac{\sigma_s\,s}{L} = \sigma_s\left(1 - \frac{s}{L}\right) = 2.48\,k\,\ln(2h/s) \qquad (2.28)$$

Elastic spreading of the loads will occur at an angle of about 45°, thus for first plastic flow, it follows from the geometry of Figure 1:

$$L \approx 2\,h + s \qquad \text{or:} \qquad h \approx \frac{(L-s)}{2} \tag{2.29}$$

Substitution of h (equation (2.29)) in equation (2.28) yields:

$$\sigma_s\left(1-\frac{s}{L}\right) = 2.48\;k\;\ln\left(\frac{2\,(L-s)}{2\,s}\right) = \sigma_s\left(1-\frac{s}{L}\right) = 2.48\;k\;\ln\left(\frac{L}{s}-1\right) \tag{2.30}$$

Rearranging of equation (2.30) results in equation (2.31):

$$\sigma_s = \frac{2.48\;k\;\ln\left(\frac{L}{s}-1\right)}{\left(1-\frac{s}{L}\right)} \;\Rightarrow\; \frac{2.48\;k\;\ln\left(\frac{L}{s}-1\right)}{\left(\frac{L-s}{L}\right)} \;\Rightarrow\; \frac{2.48\;k\;\ln\left(\frac{L}{s}-1\right)}{\left(\frac{(L/s)-1}{L/s}\right)} \tag{2.31}$$

It can be shown with general mathematics (power law approximation of a function) that this function for σ_s is nearly proportional with $\sqrt{(L/s)}$, with 2.48k being a constant. Therefore this equation can be rewritten defining a new variable C (which appears to represent a constant and shown below), which equals:

$$C = \ln\left(\frac{L}{s}-1\right)\frac{\sqrt{L/s}}{L/s-1} \tag{2.32}$$

With equations (2.31) and (2.32) one obtains equation (2.33), which can be regarded as a general form for a function being proportional with $\sqrt{(L/s)}$: A=constant x $\sqrt{(L/s)}$:

$$\sigma_s = 2.48\;k\;\ln\left(\frac{L}{s}-1\right)\frac{L/s}{(L/s)-1} = 2.48\;k\;C\;\sqrt{L/s} \tag{2.33}$$

The fact that the function C is indeed a constant in the region of interest can be noticed from figure 8, where a chart is plotted for C as function of x=(L/s)-1. The function C x $\sqrt{(L/s)}$ is given as well to show that the varying part of equation (2.31) is indeed proportional to $\sqrt{(L/s)}$ and therefore can be approximated by C $\sqrt{(L/s)}$. From figure 8 it follows that C ≈ 0.78.

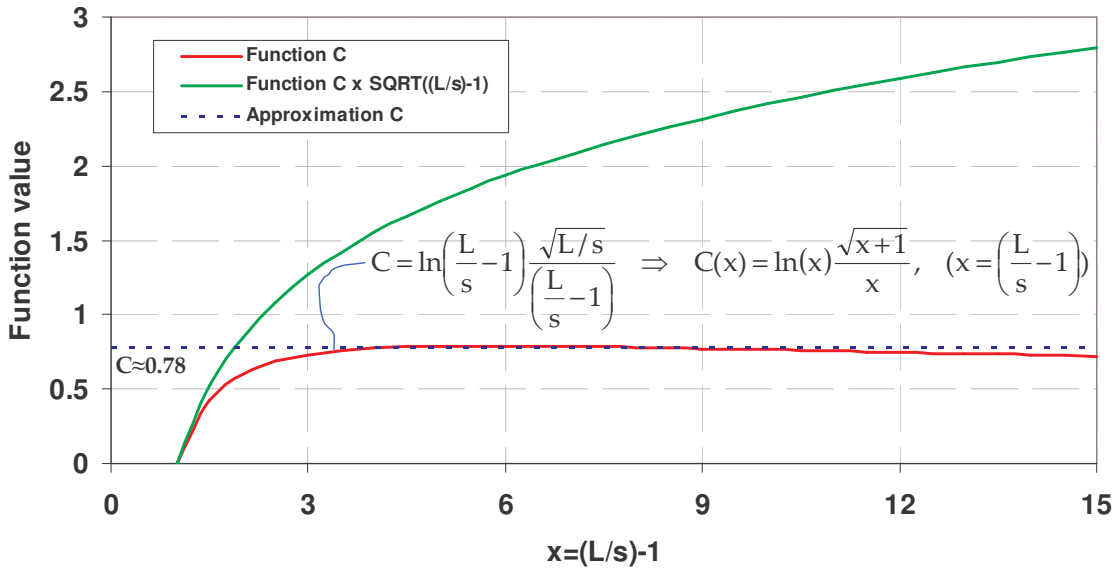

Figure 8: Function C and its approximation

The value of k, the maximum shear stress, follows from the compression test (cubic specimen), with $\sigma_1 = f_{c;90}$ and $\sigma_2 = 0$, or with Mohr's circle: $k = f_{c;90}/2$. With the nearly constant value $C \approx 0.78$ one obtains:

$$\sigma_s = 2.48\, k\, C \sqrt{L/s} = 2.48 \cdot \frac{f_{c;90}}{2} \cdot 0.78 \sqrt{L/s} = 0.97\, f_{c;90} \sqrt{L/s} \approx \mu\, f_{c;90} \sqrt{L/s} \qquad (2.34)$$

The theoretical derivation shows that $\mu = 0.97$, what is approximately 1.0. In equation (1.1) this coefficient $\mu = 1.08$, which is calculated from tests by for instance Suenson (see Kollmann [6]). Adapting the value 1.0 thus provides a lower bound approach, because apparently the real slip-lines give a higher value, and therefore gives the possibility to adapt the model to test results and to derive design rules.

3 Bearing strength of locally loaded blocks

In Van der Put [10] compression tests are analyzed from which the angle of spreading is calculated, for instance from the tests reported by Suenson (see Kollmann [6]). From these tests it follows that the maximum spreading angle is nearly 1:1.5 (≈34°). In these tests the ultimate compressive strains are approximately 15%, which is very high. The increased spreading length is probably caused by friction between timber and bearing plates, which is a result of the very high local compression stresses, and thus plasticity. Until plastic flow occurs in the specimen, the angle appears to be about 1:1 (=45°). The angle thus strongly depends on the deformation (elastic or strong plasticity).

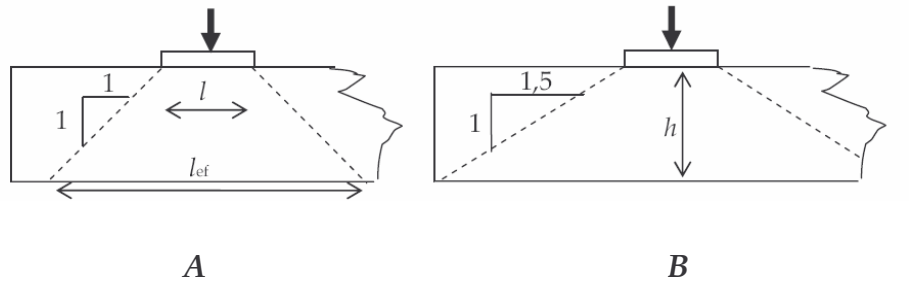

Figure 9: The angle of spreading for a) small and b) large deformations (From: Leijten and Schoenmakers [7])

As shown in Leijten and Schoenmakers [7] the failure load predictions by the model of Van der Put are much better than the empirical based Eurocode 5 [4]. In Figure 10 a chart is depicted where the model and the Eurocode 5 [4] are compared with test data by Suenson, Graf, Korin, Riberholt, and Augustin and Schikhofer. In contrast to Van der Put [10] the spreading is consistently 1:1.5, and it is demonstrated the model is of great value. In most cases μ was set to be μ = 1.0, but in some cases μ = 1.1 (≈ 1.08) provides better results in comparison with tests. The maximum compressive strength was evaluated from cubic test specimens reported by Suenson, and was taken as the reference strength for both models.

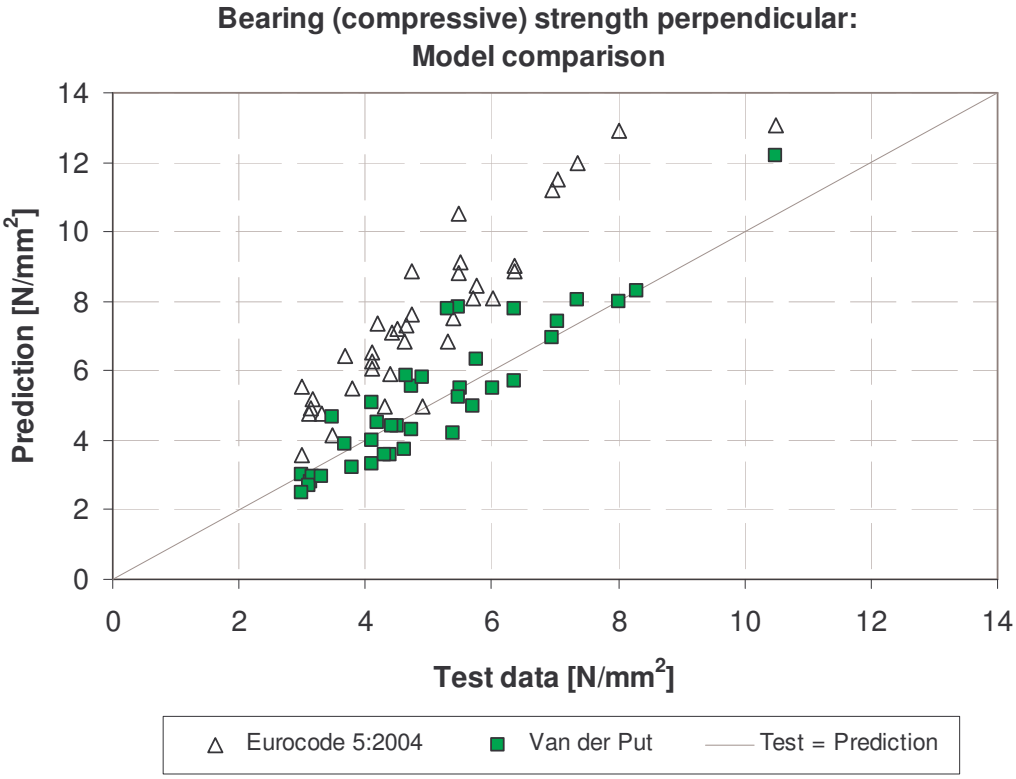

Figure 10: Evaluation of compression test data: Model comparison (From: Leijten and Schoenmakers [7])

4 Bearing strength of dowel-type joints

As mentioned previously, the model is valid for connections with dowel-type fasteners as well, but only if the embedment strength of the timber is governing failure. Splitting failure is a completely different failure mechanism where conventional stress analyses probably aren't able to describe and explain the phenomenon sufficiently accurate.

As can be noticed from Figure 2, the fastener can be regarded as the upper bearing plate and in that respect the compression test and the embedding test are related. Recall equation (1.1), with $\mu = 1.0$:

$$f_s = \mu\, f_{c;90} \sqrt{\frac{L\,t}{s\,t}} = f_{c;90} \sqrt{\frac{L\,t}{s\,t}} \quad \Rightarrow \quad f_s = f_{c;90} \sqrt{\frac{A_{lower}}{A_{upper}}} \tag{1.1}$$

In principle, the square root ratio denotes the ratio between the supporting area, L t, and the loading area, s t. In this equation the timber is a prism with a uniform width, t, and therefore t vanishes from the equation.

In the case of dowel type fasteners, distinction can be made concerning the penetration length. Usually, dowels and bolts penetrate the entire cross-section, and therefore distribute the bearing stresses beneath the fasteners uniform over the timber width. Nails, however, generally don't penetrate the full cross sectional width, and therefore the bearing stresses don't develop over the full width. The same counts for a very slender bolt that plastically deforms at ultimate bearing. In this case the highest bearing stresses occur near the shear planes in contrast to the middle part. In Figure 12 these situations are depicted.

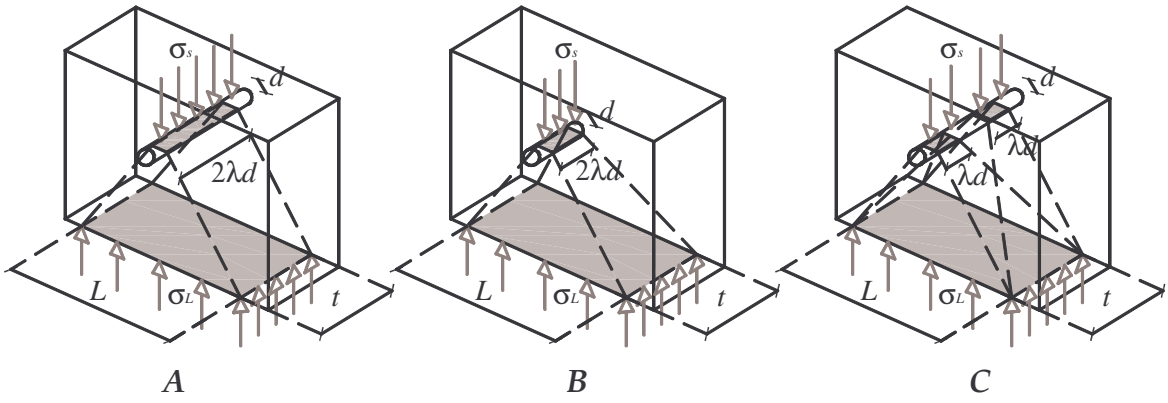

Figure 12: Different bearing lengths for different fastener behaviour / type:
A) Rigid, remains straight, B) Nail, limited penetration, C) Slender, bending

Generally, the difference between these situations is the length over which bearing stresses develop. Let this load-bearing length be denoted as 2λd, and with equation (1.1), one obtains (with s = d, being the length of the upper "bearing plate") equation (4.1), see Figure 12 as well.

$$f_s = f_{c;90} \sqrt{\frac{A_{lower}}{A_{upper}}} = f_{c;90} \sqrt{\frac{L\ t}{d\ 2\lambda d}} \qquad (4.1)$$

According to the European Yield Model, proposed in 1949 by Johansen [5], the failure load of a rigid dowel in double shear can be estimated with (Johansen I):

$$F_{u;EYM} = 2\ f_h\ d\ \frac{t}{2} \quad \Rightarrow \quad 2\ f_h\ d\ \lambda d \quad \Rightarrow \quad (t = 2\ \lambda d) \qquad (4.2)$$

In this equation $F_{u;EYM}$ is the total failure load (2 times the load per shear plane), with f_h the embedding strength, d the fastener diameter, t/2 the effective timber width because a dowel can only transfer embedding stresses over half the timber width, and 2λd the effective length (or bearing length) of the fastener. This bearing length in this situation is equal to the timber width t, see Figure 13 as well.

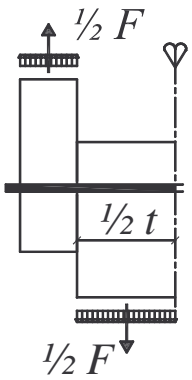

Figure 13: Johansen I

Usually, the embedment strength is defined empirically in a way that the EYM provides sufficiently accurate results. But it is well known that the embedding strength of timber perpendicular to the grain shows hardening and as so, joints designed according to the EYM are always over-designed. The embedding strength, or better called bearing strength, described in this paper (as well as in the papers by Van der Put and Leijten [11]) is denoted as f_s, according to equation (4.1) for connections.

Substitution of equation (4.1) in equation (4.2) yields (replacement of the wrong embedment strength by the correct bearing strength):

$$F = 2\ f_{c;90} \sqrt{\frac{L\ t}{d\ 2\lambda d}}\ d\ \lambda d \qquad (4.3)$$

If n fasteners are used next to each other, the failure load of equation (4.2) should become, where it is assumed that all fasteners contribute to load transfer equally ($n=n_{ef}$):

$$F_{u;EYM} = n\ 2\ f_h\ d\ \frac{t}{2} \quad \Rightarrow \quad n\ 2\ f_h\ d\ \lambda d \qquad (4.4)$$

In Figure 14 a connection with 2 rigid dowels is depicted, from which it can be noticed that the spreading length per fastener is L/n, and thus yields:

$$F = 2\ n\ f_{c;90} \sqrt{\frac{L\ t}{n\ d\ 2\lambda d}}\ d\ \lambda d \qquad (4.5)$$

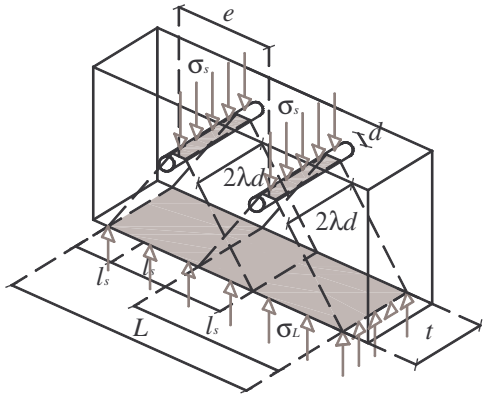

Figure 14: 2 rigid dowels next to each other, spacing e

Rewriting of this equation results in equation (4.6):

$$F = f_{c;90} \sqrt{\frac{2^2 n^2\ L\ t\ d^2\ \lambda^2 d^2}{n\ d\ 2\lambda d}} \quad \Rightarrow \quad F = f_{c;90} \sqrt{2n\ L\ t\ d\ \lambda d} \qquad (4.6)$$

In the case of rigid dowels, that is, if $2\lambda d = t$, the strength can be given by equation (4.7):

$$F = f_{c;90} \sqrt{2n\ L\ t\ d\ \frac{t}{2}} = t\ f_{c;90} \sqrt{n\ L\ d} \qquad (4.7)$$

In the case of non-rigid or short fasteners, $2\lambda d < t$, one obtains:

$$F = f_{c;90} \sqrt{2n\ L\ t\ d\ \lambda d} \quad \Rightarrow \quad F = d\ \sqrt{n\ L\ t} \sqrt{2\ \lambda}\ f_{c;90} \quad \Rightarrow \quad d\ \sqrt{n\ L\ t}\ f^*_{c;90} \qquad (4.8)$$

The factor $f^*_{c;90}$ thus is equal to $f_{c;90}\sqrt{2\lambda}$, and if λ is set to be at least t/2d (as depicted before), one obtains:

$$f^*_{c;90} = \sqrt{2\,\lambda}\, f_{c;90} = \sqrt{2\left(\frac{t}{2d}\right)}\, f_{c;90} = \sqrt{\frac{t}{d}}\, f_{c;90} \qquad (4.9)$$

what can be considered as a rule, by definition.

The only parameter not discussed is the spreading length L. As mentioned in the previous chapter and confirmed by tests, the angle of spreading is 1:1.5, so with Figure 2, it yields that $L = 3\, h_e$. If two fasteners next to each other are considered, this length must be increased by the spacing, $L = 3\, h_e + e$. Note that the fastener diameter is neglected in this respect, because the deviation is minor. The strength equations in all possible combinations (one or n fasteners, rigid or slender full-penetration fasteners, nails) are determined now.

Model validation

The accuracy of the model is evaluated by analyzing embedding tests perpendicular to the grain reported in Whale and Smith [12] (CEC). Tests have been conducted on European Whitewood, European Redwood and Canadian Spruce Pine Fir using nails with varying diameter {2.65, 3.35, 4.00, 5.00, 6.00 [mm]} and bolts {8.0, 12.0, 16.0, 20.0 [mm]}. The specimen dimensions are related to the fastener diameter as indicated in Figure 15.

These tests however are not in accordance with EN 383 [1] (1993) as the embedding strength was defined as the stress level associated with 2.1 mm displacement. However, stiffness parameters describing the load-slip behaviour are reported as well and with a generalized 3-parameter exponential function the behaviour is expressed mathematically. Evaluation of all tests with this expression indicates that plasticity did occur and the model presented here can be applied, as depicted in Figure 16.

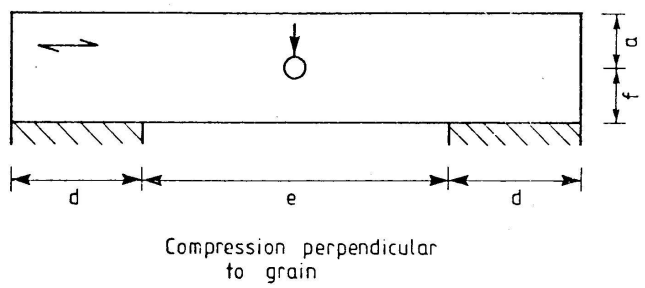

	Nails	Bolts
a	5 d	1.5 d
d	20 d	20 d
e	30 d	18 d
f	5 d	4 d
Thickness	2 d	2 d

Figure 15: Embedding tests conducted by Whale and Smith [12]

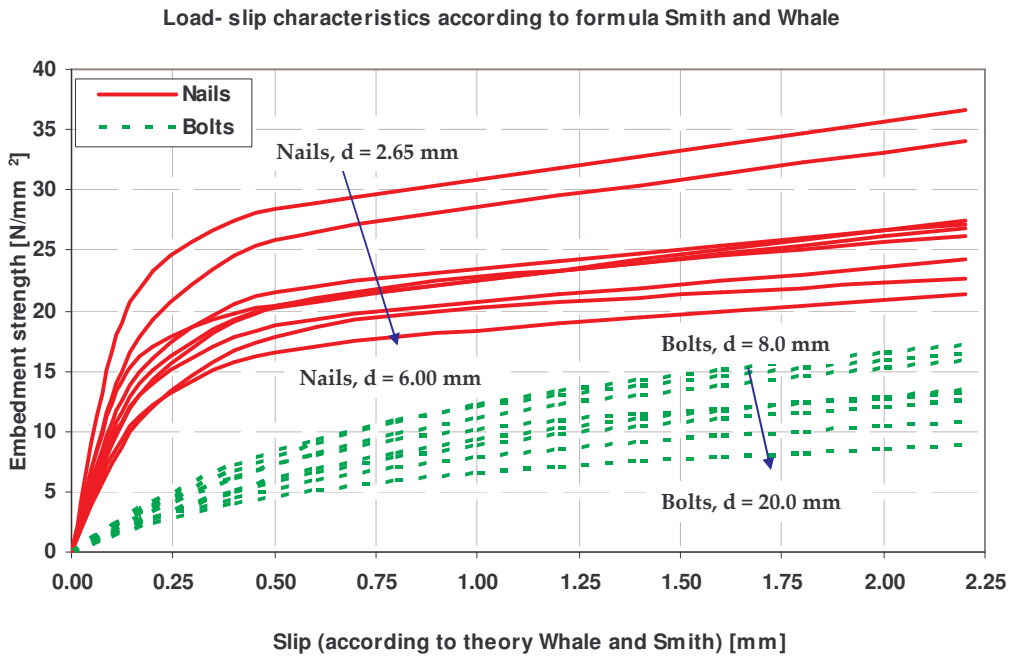

Figure 16: Load-slip behaviour according to formula of Whale and Smith [12]

Recall equation (4.5) which in the case of rigid fasteners (t=2λd) is equal to equation (4.7), with F being the embedding strength σ_h from tests on one fastener (n=1) multiplied with "t d", being the area of the "upper bearing plate":

$$F = 2\,n\,f_{c;90}\sqrt{\frac{L\,t}{d\,n\,2\lambda d}}\,d\,\lambda d = t\,f_{c;90}\sqrt{n\,L\,d} \quad \Rightarrow \quad \sigma_h\,t\,d = t\,f_{c;90}\sqrt{L\,d} \qquad (4.10)$$

With the specimen dimensions of figure 15 it follows:

$$\text{Nails:} \quad \sigma_{emb}\,t\,d = t\,f_{c;90}\sqrt{3\,f\,d} = t\,f_{c;90}\sqrt{3\,(5d)\,d} \quad \Rightarrow \quad \sigma_h = f_{c;90}\sqrt{15} \qquad (4.11)$$

$$\text{Bolts:} \quad \sigma_{emb}\,t\,d = t\,f_{c;90}\sqrt{3\,f\,d} = t\,f_{c;90}\sqrt{3\,(4d)\,d} \quad \Rightarrow \quad \sigma_h = f_{c;90}\sqrt{12} \qquad (4.12)$$

The factor $f_{c;90}$ can be regarded as the equivalent compressive strength just beneath a circular fastener, because this is the value for L/d = 1 (no spreading) in equation (4.10). Although $f_{c;90}$ is dependant of the fastener diameter this is not expressed in equations (4.11) and (4.12) what can be explained by the chosen specimen dimensions. This strength parameter thus can be regarded as the reference strength (prismatic specimen with dimensions d t f), and is regarded independent of the timber density ϱ being approximately the same for these timber species (ϱ_{mean} = 404 kg/m³, C.O.V. 6%). Because the actual value of $f_{c;90}$ is not known, it can be derived from experiments according to equations (4.11) and (4.12), which leads to an apparent value. In figure 17 a graphical representation of the embedding tests

(Whale and Smith [12]) is given (average values). The presented power fit agrees very well with the test data ($R^2 \approx 0.94$), and can be approximated with equation (4.13) for both nails and bolts:

$$f_{c;90} \approx \frac{14}{\sqrt{d}} \qquad (4.13)$$

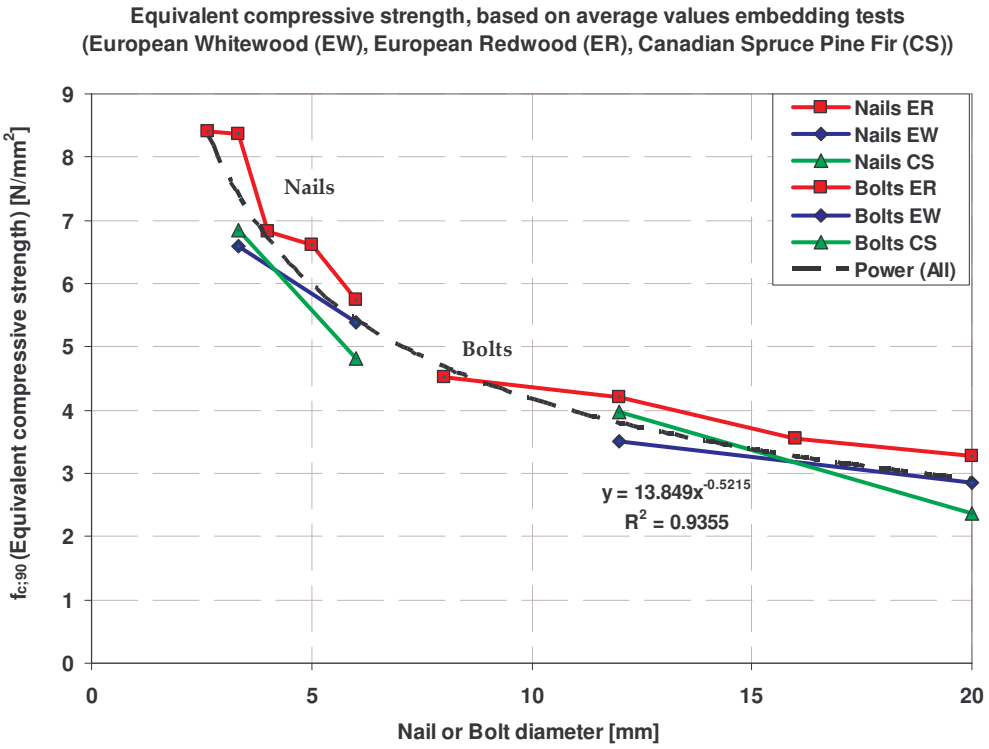

Figure 17: Equivalent compressive strength as function of fastener diameter

For comparison the embedding strengths for bolts and nails according to Eurocode 5 [4], equations (4.14) and (4.15), and the actual embedding strength from tests calculated as $f_h = F/dt$ is shown in figure 18. The characteristic density is taken as $\rho_k = 380$ kg/m^3.

Nails: $$f_{90;h} = 0{,}082\, d^{-0.3}\, \rho_k \qquad (4.14)$$

Bolts: $$f_{\alpha;h} = \frac{0{,}082\,(1-0{,}01\,d)\,\rho_k}{k_{90}\,\sin^2\alpha + \cos^2\alpha} \Rightarrow f_{90;h} = \frac{0{,}082\,(1-0{,}01\,d)\,\rho_k}{1.35+0.015\,d} \qquad (4.15)$$

In these equations d is the fastener diameter, ρ_k the characteristic timber density, α is the angle with the grain and the factor k_{90} depends on the timber density. For the species considered ($\rho_k < 500$ kg/m3) $k_{90} = 1.35 + 0.015$ d. In figure 18 the embedding strengths for both nails and bolts are approximated with one single power fit (thus not in accordance with Eurocode 5 [4]).

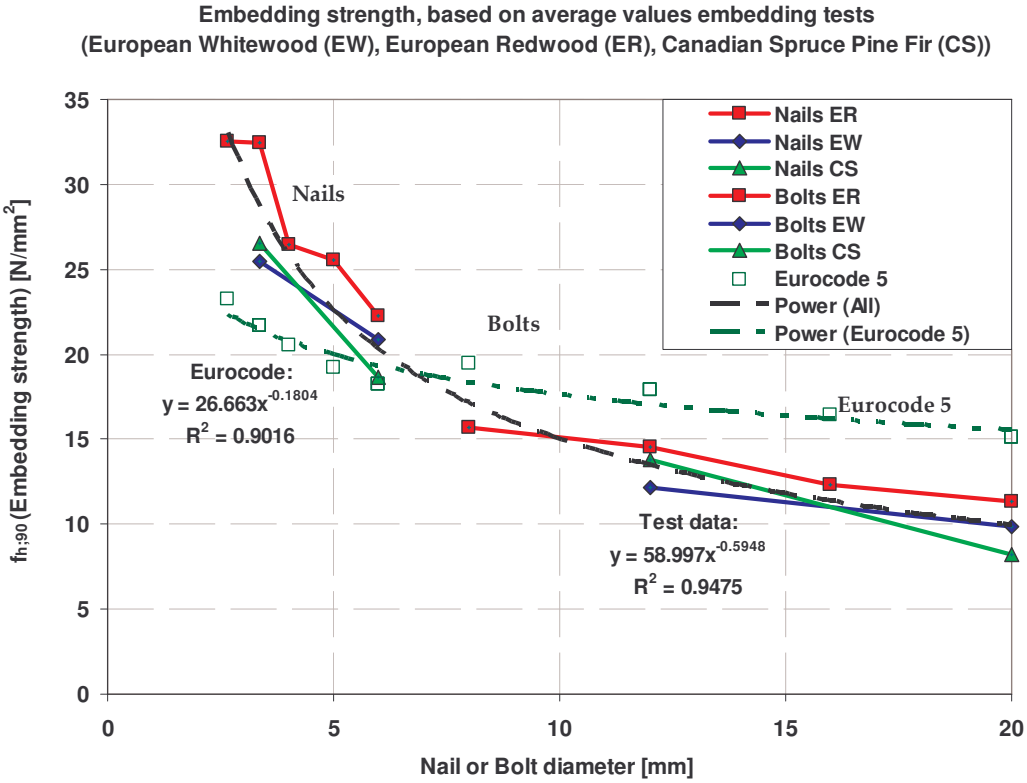

Figure 18: Embedding strength as function of fastener diameter

From the figure it is concluded that the embedding strength according to Eurocode 5 [4] doesn't describe the experiments well. For ϱ_k = 380 kg/m^3 the embedding strength of bolts is overestimated while for nails this strength is estimated too low. The prediction ability doesn't increase significantly if nails and bolts are treated separately. The power fit of the experiments shows that embedding data can be described accurately with only one equation for both nails and bolts.

The trends described by the power fit of $f_{c;90}$ (Figure 17) and $f_{h;90}$ (Figure 18) are rather similar. Therefore it is concluded that the model presented here is able to describe the tests accurately. From these figures it follows that the bearing strength of dowel type fasteners perpendicular to the grain is strongly dependant on the dowel diameter.

Conclusions

A theoretical model is derived and presented, based on the equilibrium method, which explains test results of compression tests perpendicular to the grain of timber blocks and embedding tests with dowel type fasteners. Concerning bearing blocks it is concluded that the prediction according to this model agrees better with test results than the current Eurocode 5 [4]. Concerning embedding tests with

dowel-type fasteners it is concluded that the strength can be described accurately with the model, while the current Eurocode 5 [4] doesn't. Besides, only one equation is needed for tests on both nails and bolts instead of two according to Eurocode 5 [4]. Because the embedding strength calculated as F/dt from tests is much higher for small diameter fasteners, such joints in practice will always be over designed considerably.

Acknowledgement

This research is supported by the Dutch Technology Foundation STW, applied science division of NWO and the Technology Program of the Ministry of Economic Affairs, for which the author wishes to acknowledge.

References

[1] *EN383: Timber Structures. Test methods. Determination of embedding strength and foundation values of dowel type fasteners*. 1993,

[2] Augustin, M. and Schickhofer, G.: *Behavior of glulam in compression perpendicular to grain in different strength grades and load configurations*. Proceedings of CIB-W18 / paper 39-12-6, 2006, Florence, Italy.

[3] Chakrabarty, J.: *Theory of Plasticty*. 3rd edition, 2006, Elsevier Butterworth-Heinnemann, Amsterdam, the Netherlands. ISBN: 0-7506-6638-2.

[4] Comité Européen de Normalisation (CEN): *EN 1995-1-1: 2004: Eurocode 5 - Design of timber structures. Part 1.1: General rules and rules for buildings*. 2004, CEN, Brussels, Belgium.

[5] Johansen, K.W.: *Theory of timber connections*. International Association of Bridge and Structural Engineering, Publication 9, 1949, Basel, Switzerland.

[6] Kollmann, F.: *Technologie des Holzes der Holzwerkstoffe*. Zweiter Band, 1955, Munich, Germany,

[7] Leijten, A.J.M. and Schoenmakers, J.C.M.: *Bearing strength perpendicular to the grain of locally loaded timber blocks*. Proceedings of CIB-W18 / paper 40-6-1, 2007, Bled, Slovenia.

[8] Schwarz, H.: *Die Grenztragfähigkeit des Baugrundes bei Einwirkung vertikal gezogener Ankerplatten als Zweidimensionales Bruchproblem*. 1969, Dissertation, Universität Stuttgart, Stuttgart, Germany.

[9] Van der Put, T.A.C.M.: *Explanation of the Embedding Strength of Particle Board*. Stevin report HSC-6, 1988, Delft, the Netherlands, Faculty of Civil Engineering, Delft University of Technology.

[10] Van der Put, T.A.C.M.: *Derivation of the bearing strength perpendicular to the grain of locally loaded timber blocks*. Publication of Delft Wood Science Foundation, 2006, www.DWSF.nl.

[11] Van der Put, T.A.C.M. and Leijten, A.J.M.: *Evaluation of perpendicular to grain failure of beams caused by concentrated loads of joints*. Proceedings of CIB-W18 / paper 33-7-7, 2000, Delft, The Netherlands.

[12] Whale, L.R.J. and Smith, I.: *Mechanical Joints in Structural Timberwork - Information for Probabilistic Design*. Timber Research and Development Association, 1986, Buckinghamshire, England.